Supplemental Material: Anisotropic expansion of a thermal dipolar Bose gas

Y. Tang,[1,2] A. G. Sykes,[3] N. Q. Burdick,[2,4] J. M. DiSciacca,[2,4] D. S. Petrov,[3] and B. L. Lev[1,5,4]

[1]*Department of Physics, Stanford University, Stanford CA 94305*
[2]*E. L. Ginzton Laboratory, Stanford University, Stanford CA 94305*
[3]*LPTMS, CNRS, Univ. Paris Sud, Université Paris-Saclay, 91405 Orsay, France*
[4]*Department of Applied Physics, Stanford University, Stanford CA 94305*
[5]*E. L. Ginzton Laboratory, Stanford University, Stanford CA 94305*

(Dated: September 12, 2016)

Experimental details

We perform absorption imaging using resonant 421-nm light after 16 ms of time-of-flight (TOF). To image ^{162}Dy and ^{164}Dy atoms in their ground state $|J=8, m_J=-8\rangle$, we drive σ^- transitions to ensure maximal signal-to-noise ratio, which requires a quantization field along $\hat{y}$ because our imaging beam is along $\hat{y}$. For aspect ratio (AR) measurements with the magnetic field along $\hat{z}$, we keep the field along $\hat{z}$ for the first 5 ms of TOF and then rotate to $\hat{y}$ for imaging. We experimentally find that after 5 ms the gas is sufficiently dilute that the field orientation no longer affects the subsequent expansion dynamics.

We consider the following sources of systematic uncertainties in the AR measurement. (1) Camera alignment with respect to gravity. The angle between camera's $\hat{z}$ axis and gravity is 2.8°, leading to a 0.1% error. (2) Anisotropy of camera pixels. Data are not available for this error. However, we measure this error by directly imaging the output beam of a single-mode fiber on the camera, and then rotate the fiber by 90° and image again. The beam is centered on the CCD sensor and covers about 600 × 600 pixels out of the total of 1024 × 1024. By comparing the aspect ratio of the beam imaged in the two fiber orientations, we determine the pixel aspect ratio is consistent with unity up to 0.3%. (3) We find the largest systematic error to be the residual inhomogeneity (e.g., interference fringes) in the image beam optical intensity pattern. The fringe structures have a typical length scale of ∼10 μm, which is comparable to our gas size, and have a randomly varying spatial orientation. They likely arise from aberrations in various optical elements in the imaging beam path. When we image the same gas at a fixed TOF, but with different part of the imaging beam, the gas AR varies. This is most likely due to the 2D-Gaussian fit being affected by the fringes in the background. This inhomogeneity in the imaging beam introduces a systematic error of 1% to AR measurement, which we determine by measuring the AR of a gas with 1.2×10^5 ^{164}Dy atoms at the relatively high temperature of 500 nK and with the field along $\hat{y}$ to reduce the intrinsic AR anisotropy as much as possible. We repeat the measurement at eight different locations in the imaging beam and take the standard deviation of the eight measurements as this error.

Since our theory with our trap parameters predicts allowable σ_z/σ_x only in the range $\geq$1, the values of $\sigma_z/\sigma_x < 1$ in Fig. 1(b) may be due to an uncontrolled systematic shift at the ∼0.5% level. The imperfect nulling of the $T_z - T_x$ difference in Fig. 2(b) (red data points) is related to this systematic shift.

Data analysis

We fit the atomic density images to a 2D-Gaussian function to extract the gas width σ_x and σ_z:

$$f(x,y) = Ae^{-\frac{(x-x_0)^2}{2\sigma_x^2}}e^{-\frac{(z-z_0)^2}{2\sigma_z^2}} + m_x x + m_y y + B, \quad (1)$$

where the linear terms account for the residual gradient in the background and B is the overall offset. The aspect ratio is defined as σ_z/σ_x. We note that the momentum distribution after the expansion deviates from an exact 2D-Gaussian function under the influence of Bose-enhancement, mean-field interaction, and hydrodynamic effects. Nevertheless, we find a 2D-Gaussian fit is sufficiently accurate and robust to extract the second moment of the TOF momentum distribution, allowing for a comparison to the perturbative theory discussed below. Therefore, the gas width after TOF duration t is given by

$$\sigma_i(t) = \sqrt{\sigma_{0,i}^2 + \frac{\langle p^2\rangle}{m^2}t^2}, \quad (2)$$

where $\sigma_{0,i} = \sqrt{k_{\rm B}T/m\omega_i^2}$ is the initial trap size along i.

We use the following procedure to find the best-fit scattering length a from the AR measurements made at different temperatures. First, we estimate a temperature for each AR measurement by numerically solving T_i using the following equation:

$$\sigma_i(t) = \sqrt{\sigma_{0,i}^2(T_i) + \frac{\langle p^2(T_i,a)\rangle}{m^2}t^2}, \quad (3)$$

where $i = x, z$. We assign the average of T_x and T_z to be the gas temperature. Then we calculate a χ^2 using data taken at both field orientations with the newly assigned

temperatures and the theoretical AR values for the corresponding field orientation. The scattering length value a that minimizes χ^2 is the best-fit value. To determine the 1σ error of a, we vary a around its best-fit value in both directions until χ^2 increases by 1 [1].

The best-fit a value minimizes the discrepancy between the apparent temperatures $|T_z - T_x|$. We use this fact to determine the scattering lengths for the AR data taken near the 5.1-G Feshbach resonance. For each AR measurement, we numerically find the scattering length a that yields the same T_x and T_z. We note that a has two solutions; one must choose the most appropriate solution for each field value. At fields below the resonance center, which is defined as the field with minimum atom number in the high-resolution atom-loss spectrum, we choose the large positive solution as opposed to the large negative solution. From these data points, we estimate the resonance width ΔB, which guides us in choosing the appropriate solution for points immediately above the resonance center according to $a(B) = a_{bg}[1 - \Delta B/(B - B_0)]$. We then fit all a values to this functional form and extract the final fitted ΔB.

Scattering length values

The best-fit scattering length results from this work are $a_{162} = 154(22)a_0$ for ^{162}Dy and $a_{164} = 96(22)a_0$ for ^{164}Dy, where a_0 is the Bohr radius. While a_{164} is consistent with our previous measurement from cross-dimensional relaxation experiments, a_{162} is larger than the previous value $122(10)a_0$ [2]. (Note that no value for a_{162} yet exists from Feshbach data. Also note the erratum, Ref. [3] below, for Ref. [2].)

We summarize the new and old results in Fig. S1. The new result is shown as the red data point. In our previous cross-dimensional relaxation work, we obtained five independent measurements of scattering lengths for ^{162}Dy by measuring the rethermalization time at three different field orientations [2]. Then we reported the weighted average scattering length [4]. The newly measured a_{162} is more consistent with measurements 1 and 2 from the previous work, where the field is along $\hat{z}$. The weighted average scattering length value $\bar{a}$, including all measurements, is $\bar{a}_{162}/a_d = 0.65(5)$ for ^{162}Dy and $\bar{a}_{164}/a_d = 0.47(4)$ for ^{164}Dy, corresponding to $\bar{a}_{162} = 126(10)a_0$ and $\bar{a}_{164} = 92(8)a_0$; $\bar{a}_{162}$ ($\bar{a}_{164}$) is $4a_0$ larger than (same as) the value reported in Ref. [2], and with the same errors.

Using the newly measured scattering lengths, we calculate the Knudsen parameter η for trap parameters used for taking the data in Fig. 1. The Knudsen parameter is defined as the ratio of the mean-free-path λ_i to the trap size l_i, $\eta = \frac{\lambda_i}{l_i}$, where $\lambda_i = (\sqrt{2} n_0 \sigma_{\rm tot})^{-1}$, $l_i = \sqrt{2kT(m\omega_i^2)^{-1}}$, n_0 is the peak density, $\sigma_{\rm tot}$ is the total collision cross section, and $i = x, y, z$ [5]. For magnetic atoms, $\sigma_{\rm tot}$ includes both the s-wave collision and the elastic dipolar scattering cross section [6]:

$$\sigma_{\rm tot} = \sqrt{(8\pi a^2)^2 + (2.234 a_d^2)^2}. \quad (4)$$

The criteria for the hydrodynamic regime is $\eta \ll 1$. For our ^{162}Dy gas at $T = 200$ nK, we have $[\eta_x, \eta_y, \eta_z] = [0.37, 0.17, 0.92]$, and for the ^{164}Dy gas at the same temperature, we have $[\eta_x, \eta_y, \eta_z] = [0.72, 0.33, 1.79]$. For both isotopes, the gas lies in the collisionless–hydrodynamic crossover regime.

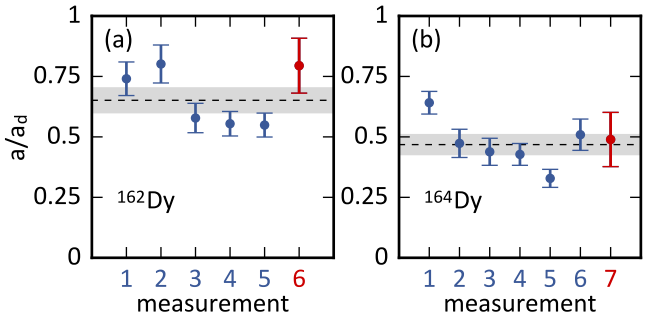

FIG. 1. Summary of scattering lengths measured from previous cross dimensional relaxation work and our current work for (a) ^{162}Dy and (b) ^{164}Dy. The blue points are from the previous work and the red point is from the current work. The dashed line marks the weighed average and the gray band represents 1σ error [4].

Theory

Introduction: We begin with the full kinetic equation for the phase-space distribution function of a fluid

$$Df(\mathbf{r}, \mathbf{p}, t) = I[f], \quad (5)$$

where

$$D \equiv \frac{\partial}{\partial t} + \frac{\mathbf{p}}{m} \cdot \nabla_{\mathbf{r}} + \mathbf{F} \cdot \nabla_{\mathbf{p}}. \quad (6)$$

Interactions are contained within both the collision functional, $I[f]$, and mean-field forces, $\mathbf{F}$. In our notation, the phase-space distribution is normalized such that $\int \frac{d^3\mathbf{p}}{h^3} f(\mathbf{r}, \mathbf{p}) = n(\mathbf{r})$, where $n(\mathbf{r})$ is the position space number-density and h is Planck's constant. To describe the expansion dynamics, no external (trapping) forces are imposed on the gas (for $t > 0$), and $\mathbf{F}$ comes purely from the mean field. That said, the trap will define the initial condition $f(\mathbf{r}, \mathbf{p}, t = 0)$.

Without interactions, the expansion of the gas is determined by

$$\partial_t f_0(\mathbf{r}, \mathbf{p}, t) + \frac{\mathbf{p}}{m} \cdot \nabla_{\mathbf{r}} f_0(\mathbf{r}, \mathbf{p}, t) = 0, \quad (7)$$

which has the important general solution $f_0 = g_0(\mathbf{p}) g_1(\mathbf{r} - \frac{\mathbf{p}}{m} t)$, where g_0 and g_1 are differentiable functions. More directly relevant to a situation where the

initial state is that of thermal equilibrium with a temperature well above degeneracy, we have the specific solution

$$f_{\rm MBE}^{(\mu,T)} = e^{\frac{\mu}{k_{\rm B}T}} \prod_{i=\{x,y,z\}} e^{-\frac{p_i^2/m + m\omega_i^2(r_i - p_i t/m)^2}{2k_{\rm B}T}}, \quad (8)$$

which corresponds exactly to the Maxwell-Boltzmann initial condition at $t = 0$ with chemical potential μ and temperature T. (The subscript MBE refers to *Maxwell-Boltzmann expansion.*) By integrating over momentum, Eq. (8) leads to the density distribution expanding as a Gaussian with time dependent standard deviations along each axis $\sigma_i(t) = \sqrt{k_{\rm B}T/m\omega_i^2}\sqrt{1+\omega_i^2 t^2}$. With regard to the more intuitive physical description we present in the main text, we point out that this expansion in Eq. (8) can be thought of as describing a *wind* which, at a specific location $\mathbf{r}$ and time t, *blows* with velocity components

$$v_i \coloneqq \langle p_i/m \rangle = \frac{r_i \omega_i^2 t}{1+\omega_i^2 t^2}, \quad (9)$$

where $i = x, y, z$, and the angular brackets denote the *momentum-averaged value as a function of position*, defined for instance by

$$\langle \mathbf{p} \rangle = \frac{1}{n(\mathbf{r},t)} \int \frac{d^3\mathbf{p}}{h^3} f(\mathbf{r},\mathbf{p},t)\mathbf{p}. \quad (10)$$

Now it is straightforward to calculate the widths (second-moments) of the momentum distribution, with this *wind* in Eq. (9) subtracted off, i.e., in the *local* rest frame of the gas. This yields

$$\langle (p_i - m v_i)^2 \rangle = \frac{m k_{\rm B} T}{1+\omega_i^2 t^2}, \quad (11)$$

thereby establishing the formal equivalence (within this *local* reference frame) to a hypothetical scenario in which a gas has anisotropic temperature $\tilde{T}_i = T/(1+\omega_i^2 t^2)$, as discussed in the main text.

The Maxwell-Boltzmann solution of Eq. (8) remains useful in a situation where the temperature is approaching degeneracy due to the fact that the Bose-Einstein distribution can be expanded as a series of Maxwell distributions with decreasing temperatures, i.e.,

$$f_{\rm BEE}^{(\mu,T)} = \sum_{n=1}^{\infty} f_{\rm MBE}^{(\mu,\frac{T}{n})}, \quad (12)$$

where the subscript BEE refers to *Bose-Einstein expansion.* The chemical potential μ in Eqs. (8) and (12) is fixed by normalizing the phase-space distribution in the manner mentioned beneath Eq. (6).

Mean-field interactions: To include interactions, we first begin with the mean-field forces. During expansion both Hartree and Fock mean-field potentials contribute to pressure in the gas and their expressions are given by

$$U_{\rm H}(\mathbf{r}) = \int d^3\mathbf{r}'\, V_{\rm int}(\mathbf{r}-\mathbf{r}')n(\mathbf{r}') \quad (13)$$

$$U_{\rm F}(\mathbf{r},\mathbf{p}) = \int \frac{d^3\mathbf{k}'}{(2\pi)^3}\, \tilde{V}_{\rm int}(\mathbf{k}-\mathbf{k}')f(\mathbf{r},\hbar\mathbf{k}'), \quad (14)$$

where wave-number and momenta are related by $\mathbf{p} = \hbar\mathbf{k}$. The two-body interaction potential $V_{\rm int}(\mathbf{r})$ is given by

$$V_{\rm int}(\mathbf{r}) = \frac{4\pi\hbar^2 a}{m}\delta^{(3)}(\mathbf{r}) + \frac{2\hbar^2 a_d}{m}\left[\frac{1-3(\hat{\epsilon}\cdot\hat{r})^2}{r^3}\right], \quad (15)$$

where a is the s-wave scattering length and a_d is the dipole length, the $\hat{}$ denotes a unit vector and $\hat{\epsilon}$ points along the direction of dipole alignment. The Fourier transform of the two-body interaction potential is required in the Fock contribution, Eq. (14), and is given by

$$\tilde{V}_{\rm int}(\mathbf{k}) = \frac{4\pi\hbar^2 a}{m} + \frac{8\pi\hbar^2 a_d}{m}\left[\left(\hat{\epsilon}\cdot\hat{k}\right)^2 - \frac{1}{3}\right]. \quad (16)$$

The force arising from such momentum-dependent mean-field potentials as those in Eqs. (13) is in general given by

$$\mathbf{F} = m\frac{d}{dt}\nabla_{\mathbf{p}}U(\mathbf{r},\mathbf{p}) - \nabla_{\mathbf{r}}U(\mathbf{r},\mathbf{p}), \quad (17)$$

which, after setting $U = U_{\rm H} + U_{\rm F}$, is then inserted into the kinetic equation given in Eq. (5).

Collisions: We now consider effects that arise from two-body collisions in the gas which, under the standard assumptions of molecular chaos, can be calculated via the inclusion of the collision integral on the right hand side of Eq. (5). This is given by

$$I[f] = \int \frac{d^3\mathbf{p}_1}{h^3}\int d^2\hat{\Omega}\frac{d\sigma}{d\Omega}v_r\Big[f'f_1'(1+f)(1+f_1) - ff_1(1+f')(1+f_1')\Big], \quad (18)$$

where $f = f(\mathbf{r},\mathbf{p})$, $f_1 = f(\mathbf{r},\mathbf{p}_1)$, $f' = f(\mathbf{r},\mathbf{p}')$, and $f_1' = f(\mathbf{r},\mathbf{p}_1')$ introduce the four momenta (two incoming and two outgoing) associated with a two-body collision, and $v_r = |\mathbf{p}-\mathbf{p}_1|/m$ is the relative velocity. It is already assumed in Eq. (18) that these momenta are related by the conservation of energy and momenta, i.e., $\mathbf{p}+\mathbf{p}_1 = \mathbf{p}'+\mathbf{p}_1'$ and $p^2+p_1^2 = (p')^2+(p_1')^2$, and thus the integration over these additional momenta has been reduced to an integration over just $\mathbf{p}_1$ (the incoming momentum) and $\hat{\Omega}$ (the solid angle through which the relative momentum is rotated during the collision). It is important to note that our expression for the collision integral includes effects due to Bose-enhancement which become increasingly relevant with higher phase-space density (lower temperatures). The differential scattering cross section $\frac{d\sigma}{d\Omega}$ is crucially a function of both incoming and outgoing relative velocities, and in the case

of identical bosons scattering at low energy via the interaction potential given in Eq. (15), this can be calculated in the first-order Born approximation to be [7]

$$\frac{d\sigma}{d\Omega} = 2a_d^2 \left[\frac{(\hat{p}_r \cdot \hat{\epsilon})^2 + (\hat{p}'_r \cdot \hat{\epsilon})^2 - 2(\hat{p}_r \cdot \hat{\epsilon})(\hat{p}'_r \cdot \hat{\epsilon})(\hat{p}_r \cdot \hat{p}'_r)}{1 - (\hat{p}_r \cdot \hat{p}'_r)^2} - \frac{2}{3} + \frac{a}{a_d} \right]^2, \tag{19}$$

where $\hat{p}_r$ and $\hat{p}'_r$ denote unit vectors along the direction of relative incoming $(\mathbf{p} - \mathbf{p}_1)$ and outgoing $(\mathbf{p}' - \mathbf{p}'_1)$ momentum respectively.

Equation of change for mean values: We are not searching for a full solution to the phase-space distribution, rather just the second moment of the momentum distribution, whose evolution is derived from Eq. (5) by multiplying by p_i^2 (where $i = x, y, z$) and integrating over space and momentum. This moment is what ultimately determines the width of the expanded image after a sufficiently long period of TOF. Let χ denote the dynamical variable of interest (i.e., $\chi = p_x^2$, say). The equation of change for χ, found by multiplying Eq. (5) by χ and then integrating over $\mathbf{p}$, is given by

$$\partial_t \langle n\chi \rangle = n\langle D\chi \rangle - \nabla_{\mathbf{r}} \cdot \langle n\chi \frac{\mathbf{p}}{m} \rangle + \mathcal{C}[\chi], \tag{20}$$

where D is defined in Eq. (6). The collisional contribution can be rearranged, using the energy and momentum conservation laws, into the form

$$\mathcal{C}(\chi) = \frac{1}{2} \int \frac{d^3\mathbf{p}}{h^3} \int \frac{d^3\mathbf{p}_1}{h^3} \int d^2\hat{\Omega} \frac{d\sigma}{d\Omega} v_r \Delta\chi f f_1 (1 + f' + f'_1), \tag{21}$$

where $\Delta\chi = \chi' + \chi'_1 - \chi - \chi_1$, with $\chi = \chi(\mathbf{r}, \mathbf{p})$, $\chi_1 = \chi(\mathbf{r}, \mathbf{p}_1)$, $\chi' = \chi(\mathbf{r}, \mathbf{p}')$, and $\chi'_1 = \chi(\mathbf{r}, \mathbf{p}'_1)$. The terms inside the parentheses of Eq. (21) arise from the Bose-enhancement factors. We also average over space to find the total average, defined by

$$\langle\langle A \rangle\rangle = \frac{1}{N} \int d^3\mathbf{r} \langle A \rangle n(\mathbf{r}, t) \tag{22}$$

where N is the total particle number. This total average is a function of time only. In this way, Eq. (20) leads us to the expression

$$\partial_t \langle\langle \chi \rangle\rangle = \langle\langle \mathbf{F} \cdot \nabla_{\mathbf{p}} \chi \rangle\rangle + \frac{1}{N} \int d^3\mathbf{r} \mathcal{C}[\chi], \tag{23}$$

where we have assumed that χ is not explicitly a function of time or space (recall $\chi = p_i^2$ where $i = x, y, z$). Integrating this ordinary differential equation, and taking the limit $t \to \infty$, we find

$$\langle\langle \chi \rangle\rangle_{t\to\infty} = \int_0^\infty dt \left[\langle\langle \mathbf{F} \cdot \nabla_{\mathbf{p}} \chi \rangle\rangle + \frac{1}{N} \int d^3\mathbf{r} \mathcal{C}[\chi] \right], \tag{24}$$

which is all that we require to proceed with our perturbative solution.

Perturbative solution: Our perturbative solution operates under the assumption that the expansion of the gas is dominated by the free-expansion solution given by Eqs. (8) and (12). Under this assumption, one can simply plug these formulae into Eq. (24), and the remaining task of computing all the integrals is straight-forward, albeit arduous. We truncate the sum in Eq. (12) to $n = 2$, thus restricting ourselves to a first-order approximation of the effects due to Bose-Einstein statistics. Accordingly, we expand Eq. (21) to first order in the degeneracy parameter $N\left(\hbar\bar{\omega}/k_{\mathrm{B}}T\right)^3$. The zeroth order terms in this degeneracy parameter establish the constants $A_{0,1,2}$ of Eq. 2 in the main text, while the first order terms establish the $B_{0,1,2}$.

After some work, we find the second moment of the gas momentum is

$$\begin{aligned}
\langle p_i^2 \rangle &= m k_{\mathrm{B}} T \left[1 + \frac{N}{16} \left(\frac{\hbar\bar{\omega}}{k_{\mathrm{B}}T} \right)^3 \right] \\
&+ 2N \frac{\hbar^2 \bar{\omega}^3 m^{3/2}}{(k_{\mathrm{B}}T)^{3/2}} \left(a_d H_d^{(i)} + a H^{(i)} \right) \\
&+ 2N \frac{\hbar^2 \bar{\omega}^3 m^{3/2}}{(k_{\mathrm{B}}T)^{3/2}} \left(a_d F_d^{(i)} + a F^{(i)} \right) \\
&+ 2N m^2 a_d^2 \bar{\omega}^2 \Bigg\{ \left[A_0^{(i)} + A_1^{(i)} \left(\frac{a}{a_d} \right) + A_2^{(i)} \left(\frac{a}{a_d} \right)^2 \right] \\
&+ N \left(\frac{\hbar\bar{\omega}}{k_{\mathrm{B}}T} \right)^3 \left[B_0^{(i)} + B_1^{(i)} \left(\frac{a}{a_d} \right) + B_2^{(i)} \left(\frac{a}{a_d} \right)^2 \right] \Bigg\},
\end{aligned} \tag{25}$$

where $i = x, y, z$ denotes the axis, $\bar{\omega} = (\omega_x \omega_y \omega_z)^{1/3}$ is the geometric mean trap frequency, T is temperature, N is atom number, $a_d = \mu_0 \mu^2 m/(8\pi\hbar^2)$ is the dipole length scale, and a is the s-wave scattering length. The dimensionless constants H_d, H, F_d, F, A, and B are remnants of integration over the solid angles of incoming and outgoing momenta and are given in the appendix of this supplement. These turn out to be complicated, mainly by the expression for the differential cross section, and the easiest approach is to simply compute these numerically for a given set of trap frequencies.

The first line in Eq. (25) comes from the expansion of a non-interacting gas, including the Bose statistics, to first order in the degeneracy parameter. The second and third line are derived from the Hartree and Fock mean-field interactions, respectively. The fourth line accounts for the two-body collisional effects during expansion, and the fifth line describes the Bose-enhancement correction to the collision integral.

In addition, we have looked at results involving the full summation in Eq. (12), i.e., including effects due to the degeneracy parameter $N\left(\hbar\bar{\omega}/k_{\mathrm{B}}T\right)^3$ at all orders. In this case, the integrals associated with calculating $\langle p_i^2 \rangle$ be-

come considerably more complicated. However, we were able to compute an upper bound on $\langle p_i^2 \rangle$ by replacing the integrand with an absolute value. We found that even this upper bound contributes negligible difference compared to Eq. (25) in the temperature range of the current experiment.

Appendix: Expressions for H_d, H, F_d, F, A, and B

$$H_d^{(i)} = \frac{1}{2^3\pi^{3/2}} \int d^2\hat{p} \frac{\hat{p}_i^2}{\left(\sum_{j=\{x,y,z\}} \hat{p}_j^2 \frac{\bar{\omega}^2}{\omega_j^2}\right)^{3/2}} \left[(\hat{p}\cdot\hat{\epsilon})^2 - \frac{1}{3}\right] \tag{26}$$

$$H^{(i)} = \frac{1}{2^4\pi^{3/2}} \int d^2\hat{p} \frac{\hat{p}_i^2}{\left(\sum_{j=\{x,y,z\}} \hat{p}_j^2 \frac{\bar{\omega}^2}{\omega_j^2}\right)^{3/2}} \tag{27}$$

$$F_d^{(i)} = \frac{1}{2^3\pi^{3/2}} \int d^2\hat{p} \frac{\sqrt{\left(\sum_{j=\{x,y,z\}} \frac{\omega_j^2\hat{p}_j^2}{\omega_i^2}\right) - 1} - \arccos\left[\sqrt{\frac{\omega_i^2}{\sum_{j=\{x,y,z\}} \hat{p}_j^2\omega_j^2}}\right]}{\left[\left(\sum_{j=\{x,y,z\}} \frac{\omega_j^2\hat{p}_j^2}{\omega_i^2}\right) - 1\right]^{3/2}} \left[(\hat{p}\cdot\hat{\epsilon})^2 - \frac{1}{3}\right] \tag{28}$$

$$F^{(i)} = \frac{1}{2^4\pi^{3/2}} \int d^2\hat{p} \frac{\sqrt{\left(\sum_{j=\{x,y,z\}} \frac{\omega_j^2\hat{p}_j^2}{\omega_i^2}\right) - 1} - \arccos\left[\sqrt{\frac{\omega_i^2}{\sum_{j=\{x,y,z\}} \hat{p}_j^2\omega_j^2}}\right]}{\left[\left(\sum_{j=\{x,y,z\}} \frac{\omega_j^2\hat{p}_j^2}{\omega_i^2}\right) - 1\right]^{3/2}} \tag{29}$$

$$A_0^{(i)} = \frac{3}{2^6\pi^2} \int d^2\hat{p} \int d^2\hat{p}' \frac{(\hat{p}_i'^2 - \hat{p}_i^2)\left[\frac{(\hat{p}'\cdot\hat{\epsilon})^2 + (\hat{p}\cdot\hat{\epsilon})^2 - 2(\hat{p}'\cdot\hat{\epsilon})(\hat{p}\cdot\hat{\epsilon})(\hat{p}'\cdot\hat{p})}{1-(\hat{p}\cdot\hat{p}')^2} - \frac{2}{3}\right]^2}{\sqrt{\sum_{j=\{x,y,z\}} \hat{p}_j^2 \frac{\omega_j^2}{\bar{\omega}^2}}} \tag{30}$$

$$A_1^{(i)} = \frac{3}{2^5\pi^2} \int d^2\hat{p} \int d^2\hat{p}' \frac{(\hat{p}_i'^2 - \hat{p}_i^2)\left[\frac{(\hat{p}'\cdot\hat{\epsilon})^2 + (\hat{p}\cdot\hat{\epsilon})^2 - 2(\hat{p}'\cdot\hat{\epsilon})(\hat{p}\cdot\hat{\epsilon})(\hat{p}'\cdot\hat{p})}{1-(\hat{p}\cdot\hat{p}')^2} - \frac{2}{3}\right]}{\sqrt{\sum_{j=\{x,y,z\}} \hat{p}_j^2 \frac{\omega_j^2}{\bar{\omega}^2}}} \tag{31}$$

$$A_2^{(i)} = \frac{3}{2^6\pi^2} \int d^2\hat{p} \int d^2\hat{p}' \frac{(\hat{p}_i'^2 - \hat{p}_i^2)}{\sqrt{\sum_{j=\{x,y,z\}} \hat{p}_j^2 \frac{\omega_j^2}{\bar{\omega}^2}}} \tag{32}$$

$$B_0^{(i)} = \frac{3}{2^7\pi^2} \int d^2\hat{p} \int d^2\hat{p}' \frac{(\hat{p}_i'^2 - \hat{p}_i^2)\left[\frac{(\hat{p}'\cdot\hat{\epsilon})^2 + (\hat{p}\cdot\hat{\epsilon})^2 - 2(\hat{p}'\cdot\hat{\epsilon})(\hat{p}\cdot\hat{\epsilon})(\hat{p}'\cdot\hat{p})}{1-(\hat{p}\cdot\hat{p}')^2} - \frac{2}{3}\right]^2}{\sqrt{\sum_{j=\{x,y,z\}} (3\hat{p}_j^2 + \hat{p}_j'^2) \frac{\omega_j^2}{\bar{\omega}^2}}} \tag{33}$$

$$B_1^{(i)} = \frac{3}{2^6\pi^2} \int d^2\hat{p} \int d^2\hat{p}' \frac{(\hat{p}_i'^2 - \hat{p}_i^2)\left[\frac{(\hat{p}'\cdot\hat{\epsilon})^2 + (\hat{p}\cdot\hat{\epsilon})^2 - 2(\hat{p}'\cdot\hat{\epsilon})(\hat{p}\cdot\hat{\epsilon})(\hat{p}'\cdot\hat{p})}{1-(\hat{p}\cdot\hat{p}')^2} - \frac{2}{3}\right]}{\sqrt{\sum_{j=\{x,y,z\}} (3\hat{p}_j^2 + \hat{p}_j'^2) \frac{\omega_j^2}{\bar{\omega}^2}}} \tag{34}$$

$$B_2^{(i)} = \frac{3}{2^7\pi^2} \int d^2\hat{p} \int d^2\hat{p}' \frac{(\hat{p}_i'^2 - \hat{p}_i^2)}{\sqrt{\sum_{j=\{x,y,z\}} (3\hat{p}_j^2 + \hat{p}_j'^2) \frac{\omega_j^2}{\bar{\omega}^2}}} \tag{35}$$

Here we used the notation $\hat{p} = (\sin\theta\cos\phi, \sin\theta\sin\phi, \cos\theta)$, and $\int d^2\hat{p} = \int_0^\pi \sin\theta d\theta \int_0^{2\pi} d\phi$. See Table I for specific values pertaining to our experimental set up.

	$\omega_x : \omega_y : \omega_z = 107 : 49 : 266$		$\omega_x : \omega_y : \omega_z = 89 : 44 : 219$
	$\hat{\epsilon} = \hat{y}$	$\hat{\epsilon} = \hat{z}$	$\hat{\epsilon} = \hat{z}$
$\left\{A_0^{(x)}, A_0^{(z)}\right\}$	$\{-0.00182, 0.00608\}$	$\{0.00192, 0.00412\}$	$\{0.00166, 0.00407\}$
$\left\{A_1^{(x)}, A_1^{(z)}\right\}$	$\{0.0256, 0.0191\}$	$\{-0.0209, 0.0190\}$	$\{-0.0201, 0.0190\}$
$\left\{A_2^{(x)}, A_2^{(z)}\right\}$	$\{-0.00835, 0.0666\}$	$\{-0.00835, 0.0666\}$	$\{-0.00967, 0.0659\}$
$\left\{B_0^{(x)}, B_0^{(z)}\right\}$	$\{-0.000195, 0.000553\}$	$\{0.000206, 0.000362\}$	$\{0.000185, 0.000366\}$
$\left\{B_1^{(x)}, B_1^{(z)}\right\}$	$\{0.00253, -0.000207\}$	$\{-0.00206, 0.00155\}$	$\{-0.00201, 0.00159\}$
$\left\{B_2^{(x)}, B_2^{(z)}\right\}$	$\{-0.000934, 0.00586\}$	$\{-0.000934, 0.00586\}$	$\{-0.00104, 0.00593\}$
$\left\{H_d^{(x)}, H_d^{(z)}\right\}$	$\{-0.0176, -0.0531\}$	$\{0.000567, 0.0913\}$	$\{0.000383, 0.0893\}$
$\left\{H^{(x)}, H^{(z)}\right\}$	$\{0.0354, 0.0935\}$	$\{0.0354, 0.0935\}$	$\{0.0352, 0.0925\}$
$\left\{F_d^{(x)}, F_d^{(z)}\right\}$	$\{0.00814, 0.0150\}$	$\{-0.00946, -0.0187\}$	$\{-0.00918, -0.0181\}$
$\left\{F^{(x)}, F^{(z)}\right\}$	$\{0.0354, 0.0935\}$	$\{0.0354, 0.0935\}$	$\{0.0352, 0.0925\}$

TABLE I. Values of the integrals in the cases which pertain to our various experimental configurations.

[1] I. Hughes and T. Hase, *Measurements and their Uncertainties: A practical guide to modern error analysis* (Oxford University Press, 2010).

[2] Y. Tang, A. Sykes, N. Q. Burdick, J. L. Bohn, and B. L. Lev, "s-wave scattering lengths of the strongly dipolar bosons ^{162}Dy and ^{164}Dy," Phys. Rev. A **92**, 022703 (2015).

[3] Y. Tang, A. Sykes, N. Q. Burdick, J. L. Bohn, and B. L. Lev, "Erratum: s-wave scattering lengths of the strongly dipolar bosons ^{162}Dy and ^{164}Dy [Phys. Rev. A **92** , 022703 (2015)]," Phys. Rev. A **93**, 059905 (2016).

[4] R. C. Paule and J. Mandel, "Consensus values and weighting factors," J. Res. Nat. Bur. Stand. **87**, 377 (1982).

[5] I. Shvarchuck, Ch. Buggle, D. S. Petrov, M. Kemmann, W. von Klitzing, G. V. Shlyapnikov, and J. T. M. Walraven, "Hydrodynamic behavior in expanding thermal clouds of ^{87}Rb," Phys. Rev. A **68**, 063603 (2003).

[6] J. L. Bohn, M. Cavagnero, and C. Ticknor, "Quasi-universal dipolar scattering in cold and ultracold gases," New J. Phys. **11**, 055039 (2009).

[7] J. L. Bohn and D. S. Jin, "Differential scattering and rethermalization in ultracold dipolar gases," Phys. Rev. A **89**, 022702 (2014).